Review of Computer Engineering Research
2022 Vol. 9, No. 4, pp. 222-238.
ISSN(e): 2410-9142
ISSN(p): 2412-4281
DOI: 10.18488/76.v9i4.3168

BURIED WIRE DETECTION AND CLUSTERING ALGORITHM WITH GROUND PENETRATING RADAR

Ozkan AKBULUT[1+]
Ahmet Gungor PAKFILIZ[2]

[1]*Havelsan A.S, Turkey.*
Email: ozkanakbulut.041@gmail.com
[2]*Department of Electrical and Electronics, Baskent University, Turkey.*
Email: apakfiliz@baskent.edu.tr

(+ Corresponding author)

Article History
Received: 2 August 2022
Revised: 9 September 2022
Accepted: 29 September 2022
Published: 14 October 2022

Keywords
Buried object detection
Clustering
Gaussian mixture model
Go-Decomposition
Ground penetrating radar
K-Means
Prescreening
Wire detection.

ABSTRACT

Improvised explosive devices (IEDs) have recently become a considerable national security concern for governments due to their increased use. Since IEDs do not have a particular shape, detecting and classifying IEDs becomes a complex problem. Due to the irregularity of the wire shape, recent research focuses on detecting command wire, which is the triggering mechanism in IEDs. This study proposes a detection and clustering algorithm for wire detection. The synthetic data were generated using the gprMax software, an open-source Finite-Difference Time-Domain (FDTD) simulation environment. Different wire and clutter orientations were simulated while creating a 2D GPR database. Three different prescreening algorithms are compared concerning computational time and signal-to-noise ratio. The Go Decomposition (GoDec) method was used at the preprocessing stage. Discriminating the buried wire from clutter was conducted using the k-means clustering method. The proposed algorithm results show promising outcomes over simulated GPR 2D C-scans.

Contribution/Originality: This study focuses on detecting and discriminating the buried wire, which is the triggering mechanism of IEDs. Compared with the proven methods at the preprocessing stage, a better signal-to-noise ratio is achieved using Go Decomposition, which makes this study novel, and the buried wires are discriminated with a higher accuracy using k-means clustering than the related methods.

1. INTRODUCTION

The problem of detecting improvised explosive devices is a critical concern for governments in the developing world [1]. Irregularity of shape and contents in the structure of IEDs makes them quite hard to detect with most sensors [2].

The most popular subsurface sensors used for the identification and localization of buried objects, e.g., pipes, landmines, and IEDs, are ground penetrating radars (GPRs) [3, 4]. A GPR probes the underground surface by emitting electromagnetic (EM) waves and analyzing the return signals caused by underground anomalies. The return signal's magnitude and character depend on the geometry, the contrast in the material properties of the objects, and their surroundings [5]. Sensors' gathered signals are processed using different signal and image processing techniques [6].

Only a few pieces of research focus on the buried wire detection problem. In Yılmaz [2], the buried wire detection and classification problem are studied in detail, and the detection and classification of wires was carried

out successfully. However, the proposed algorithms are based on 3D C-scan data, which requires more computational time than real-time applications.

In Liu, et al. [7], the importance of antenna polarization for buried wire detection is studied by comparing the proposed antenna with two conventional GPR survey profiles. The results are based on hyperbolic signatures of buried wires. However, since the study focused on the hardware, the detection, clustering, or classification problem is not studied. In Heinzel, et al. [8], the unburied wire detection problem is studied with a multiple-input multiple-output (MIMO) synthetic aperture radar (SAR), and detection of thin wire is carried out successfully. Nevertheless, the buried wire problem was still not studied because the authors expected that the buried wire problem would worsen the detection results.

This study proposes a detection and clustering algorithm for buried wire detection, which has been developed based on a dataset obtained from gprMax electromagnetic modeling software [9]. The proposed algorithm has two stages. In the first stage, a prescreening algorithm was developed based on the Go Decomposition (GoDec) method. A clustering algorithm using the Gaussian mixture model was used in the second stage.

The rest of the paper is organized as follows: Section 2 presents the GPR working principle with GPR range profiles; information about the simulation setup and dataset are given in Section 3; Section 4 describes the theoretical background of the prescreening and clustering methods; Section 5 presents the proposed method; Section 6 contains the simulation results; and the conclusion and discussion regarding the algorithm are given in Section 7.

2. GPR PRINCIPLE

A ground penetrating radar (GPR) is a short-range radar system well known for subsurface inhomogeneities such as buried objects or different layers. It transmits and receives signals based on electromagnetic (EM) wave scattering principles. The EM waves propagate into the ground at a speed determined mainly by the electrical properties of the medium. A portion of the EM wave energy is reflected and captured by the receiver antenna when a change occurs in the subsurface [10]. This wave propagation of GPR is illustrated in Figure 1.

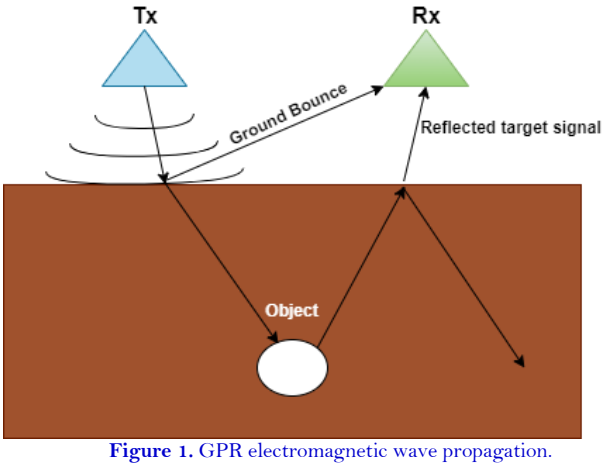

Figure 1. GPR electromagnetic wave propagation.

2.1. GPR Range Profiles

In this section, a brief definition of the GPR data outputs is given. A received reflected target signal, shown in Figure 1, is called an A-scan. Multiple A-scans that are recorded one after another in cross-track dimensions are called B-scans. A B-scan comprises two-dimensional (2D) data obtained using one transmitter and one receiver antenna moving along the track, or with an antenna array aligned with the cross-track position. A C-scan is comprises three-dimensional (3D) data that can be obtained with multiple B-scans recorded at along-track positions. Figure 2 shows the GPR range profiles and movement directions.

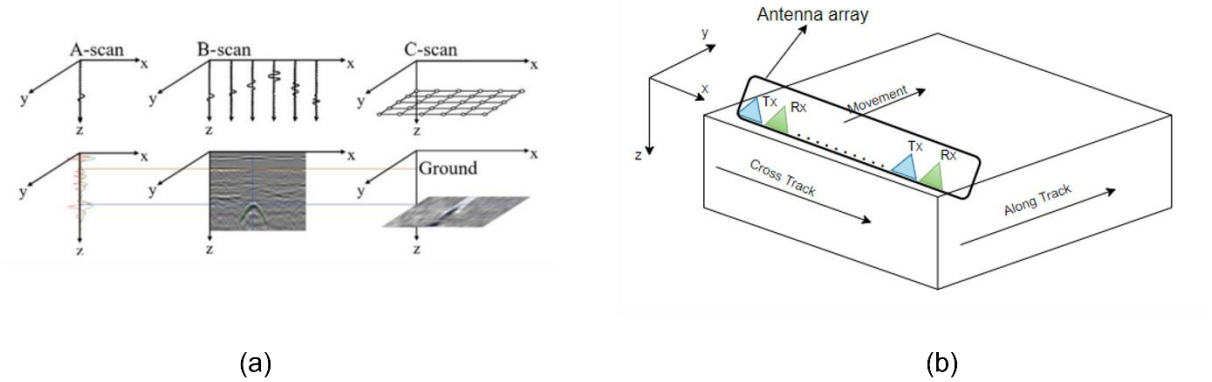

Figure 2. Definition of GPR data outputs: (a) GPR range profiles, (b) movement directions.

3. DATASET AND SIMULATION SETUP

The dataset, which contains 20 simulation scenarios, is generated using the gprMax program. Eight of these simulation scenarios are shown in Figure 3 to prevent confusion. Each scenario is scanned as shown in Figure 2b. A transmitter and receiver antenna pair is moved across along-track dimensions between 10–70 cm, which creates a B-scan. Each time the pair is finished scanning the along-track dimensions, it is moved 5 cm in the cross-track dimension and scanned again. This process is repeated 14 times in a cross-track position simulating an antenna array with 14 transmitter and receiver pairs. Thus, one C-scan consists of 14 B-scans for each scenario. In each simulation, some wires have different orientations and clutter modeled as spheres at different depths.

3D data processing can be achieved with C-scans. However, the time required to process 3D data is greater than real-time scenarios. First, a prescreening algorithm is applied to the B-scans. After that, each B-scan is decreased to 1D data based on energy calculations. Then, the data from each 1D B-scan are combined, and a 2D C-scan is achieved, as shown in Figure 2a. The features of these 2D C-scans are recorded and discriminated against using the Gaussian mixture model (GMM) clustering method.

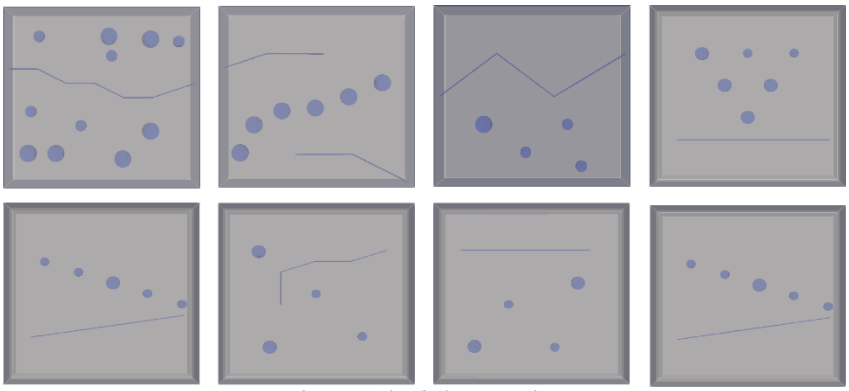

Figure 3. Simulation scenarios.

4. THEORETICAL BACKGROUND AND THE PROPOSED METHOD

A general block diagram of the proposed method for the buried wire detection problem is given in Figure 4.

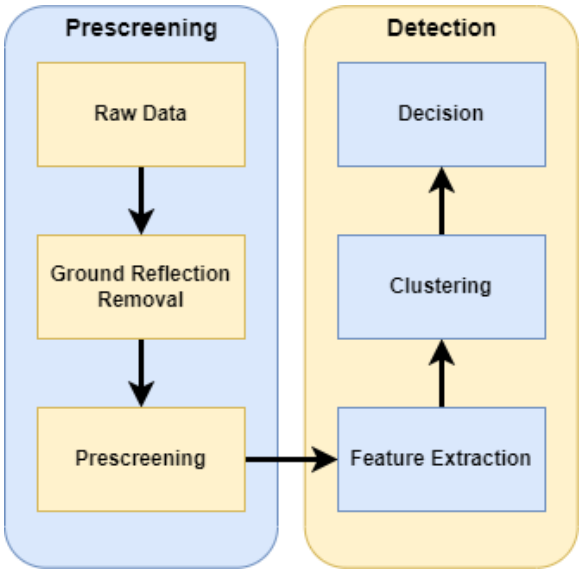

Figure 4. Block diagram of data processing.

4.1. Ground Reflection Removal

The first reflection of the GPR signal occurs during the air-to-ground transition, as shown in Figure 1. A considerable amount of the signal is reflected from the ground. This reflection dominates the B-scan and prevents targets from appearing, as shown in Figure 5 (left). Therefore, a reflection removal algorithm must be applied to the raw data.

Due to computational requirements, the removal algorithm of this reflection must be accessible and practical. The reflection time of this signal is equal to the one-way electromagnetic wave propagation, which depends on the distance between the transmitter (Tx)/receiver (Rx) antenna pair and the ground [2]. In case of a constant distance from antenna pairs to the ground, such as a ground vehicle mounted GPR, the time index of the reflection signal would always be near the same depth bins. This time index of reflection could be used as a constant gating index. However, the time index could change when the vehicle is in motion. In addition, the GPR signal reflected from the ground always has a higher value than the searched targets. Therefore, the peak of the reflection must be tracked, and the B-scan must be gated according to this peak.

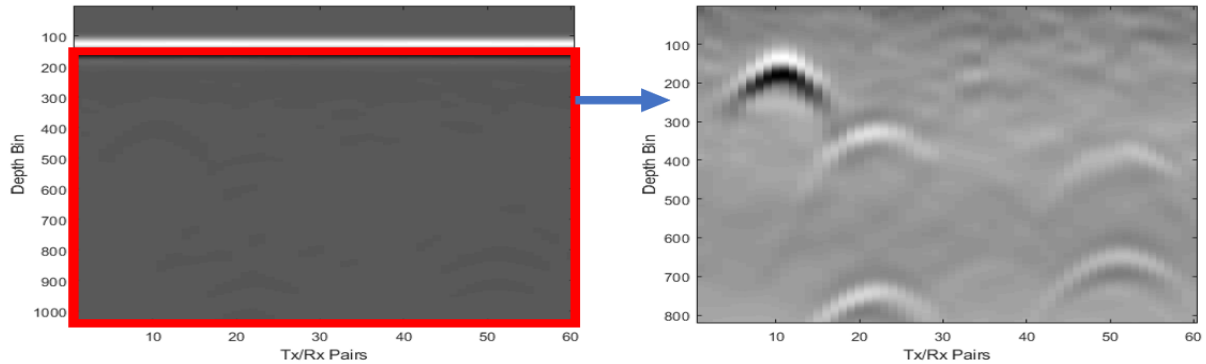

Figure 5. Ground reflection removal (raw B-scan data is on the left, and ground reflection removal is applied to the B-scan on the right).

Since the distance from the antenna to the ground would not change dramatically, the time index of the first reflection could be tracked adaptively. This tracking can be done by looking the first 200 bins of the GPR image. The image could be gated when the peak is detected, as in Figure 5 (right).

4.2. Prescreening

After the peak tracking algorithm, a prescreening algorithm is applied to the B-scans so that the background of the signal can be separated. Prescreening is also known as clutter reduction. Thus, image enhancement would be achieved, and targets would appear firmer. There are many prescreening algorithms studied with the GPR. In this study, three algorithms are studied and compared for the signal-to-noise ratio (SNR) and computational time. These algorithms are based on the statistical properties of the data and decomposition into subspaces.

4.2.1. Singular Value Decomposition (SVD)

SVD-based image enhancement is well studied in the literature. It is performed by decomposing B-scan image X (with dimensions M x N) into different spectral components using SVD, i.e.,

$$X = USV^T \quad (1)$$

where, U and V have dimensions M x M, N x N are unitary matrices, and S = *diag*(s_1, s_2, …., s_M) with $s_1 \geq s_2 \geq \ldots \geq s_M \geq 0$ are singular values of X [11].

As singular values are arranged in descending order, the first few larger singular values generally correspond to effective signals with solid correlations, while the smaller values correspond to the noise with weak correlations [12].

4.2.2. Robust Principal Component Analysis (RPCA)

Since the classical principle component analysis (PCA) is very sensitive to data outliers, the RPCA is used, which overcomes the drawbacks of the PCA for background removal. Each B-scan for the RPCA can be expressed as:

$$X = L + S + N \quad (2)$$

where L is the low-rank component, S is the sparse component, and N denotes noise. It focuses on finding a low-rank structure in high-dimensional data by solving the following optimization problem [13]:

$$\min_{L,S} ||L||_* + \lambda ||S||_1 \quad \text{subject to} \quad ||X - L - S||_F \leq \delta \quad (3)$$

where $||\ldots||_*$ denotes the nuclear norm of L (i.e., the sum of the singular values), $||\ldots||_1$ is l-1 norm of S (i.e., the sum of the absolute values of matrix entries), $||\ldots||_F$ denotes the Frobenius norm, δ is a constant parameter for noise, and λ is a regularization parameter. The low-rank component represents the slowly varying background, and the sparse component contains the local variations, which can naturally include significant variations due to target anomalies [14].

Every time a GPR-carrying vehicle moves in the along-track direction, a 2D GPR data matrix (B-scan) is obtained, as shown in Figure 2. This B-scan data matrix (**X**) consists of target responses (**S**), clutter (**L**), and noise (**N**) variables, as modeled in Equation (2). Thus, we can separate the sparse component from the ground by solving the RPCA convex optimization problem.

However, the solutions adopted in Candès, et al. [15] and Song, et al. [16] are time-consuming to some extent since they usually need more than 100 iterations to converge. To meet the speed and reliability requirements of prescreening, a more efficient and robust solution is needed [17].

4.2.3. Go Decomposition (GoDec)

In [18], the development and implementation of GoDec are explained in detail. It is an RPCA-based and faster solution technique because it can be significantly accelerated by bilateral random projections [18]. GoDec decomposes X in (2) to minimize the error as:

$$\min_{\mathbf{L},\mathbf{S}} \|\mathbf{X} - \mathbf{L} - \mathbf{S}\|_F^2 \quad \text{subject to} \quad \text{rank}(\mathbf{L}) \leq r, \quad \text{card}(\mathbf{S}) \leq k \quad (4)$$

where (L) is the rank of matrix L, and card (S) denotes the cardinality of matrix S. This method is summarized and modified in [17]. To be able to use GoDec in GPR applications, it is necessary to make some adaptions [17]. One is to decompose the focused GPR image instead of the original B-scan to enhance sparsity and target responses [16]. Therefore, GoDec is applied to the B-scans after ground reflection removal. The other is to make initial estimations for the sparse (**S**) and low-rank (**L**) matrices. In Li, et al. [19], it is said that the initial values of the low-rank and sparse matrices can accelerate the GoDec solving process.

Making initial estimations as the average of the columns of the low-rank matrix ($\mathbf{L}_0$) and subtracting $\mathbf{L}_0$ from the original data matrix (**X**) for initial sparsity ($\mathbf{S}_0$) shortens the computational time of GoDec [17] (typically less than ten iterations). The formulas for the initial estimation of the low-rank matrix and sparsity are given in Equation 5 and Equation 6.

$$L_0 = \left(\frac{1}{N}\sum_{i=1}^{N} x_i\right) 1_{N\times 1}^{T} \tag{5}$$

$$\mathbf{S}_0 = \mathbf{X} - \mathbf{L}_0 \tag{6}$$

Detecting targets from B-scans is possible. However, extracting specific targets is not that easy from B-scans. To be able to find out which target it is, it is necessary to identify certain features that cannot be extracted from B-scans for buried wire. Since wire reflections do not vary much from clutter responses, C-scan data must be studied to detect and classify the wire.

4.2.4. Comparison of Prescreening Algorithms

4.2.4.1. SNR Comparison

The signal-to-noise ratio (SNR) is a conventional method used in image processing. The SNR of an image can be measured as the ratio of the average signal (M) to the standard deviation of the noise (N) [20]. Using the image's standard deviation, the image's background and foreground do not need to be detected and processed.

$$SNR = \frac{\mu(X)}{\sigma(X)} \tag{7}$$

Where X is the B-scan data, and μ and σ are the average and the standard deviations of X, respectively.

The SNR is compared over a predefined scenario, as shown in Figure 6. This scenario is scanned as described in Section 3.

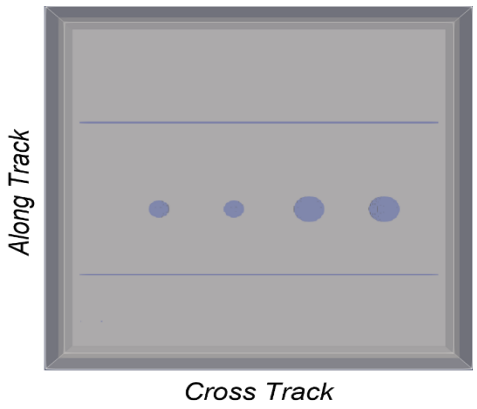

Figure 6. SNR comparison scenario.

The SNR is calculated for every B-scan that creates a C-scan and is recorded. Figure 7 illustrates that the GoDec method showed promising results compared to the other methods.

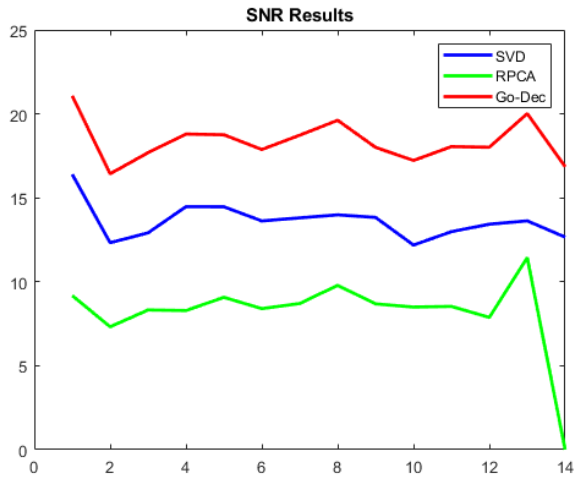

Figure 7. SNR results.

4.2.4.2. Computational Time Comparison

A time comparison is made with the same scenario used in the SNR comparison. The RPCA method is much slower than the singular value decomposition (SVD) and GoDec methods. The SVD is the fastest algorithm to work with for this study. However, the time difference between the SVD and GoDec could be ignored since the SNR of GoDec is better than the SNR of SVD. The comparison results are shown in Figure 8.

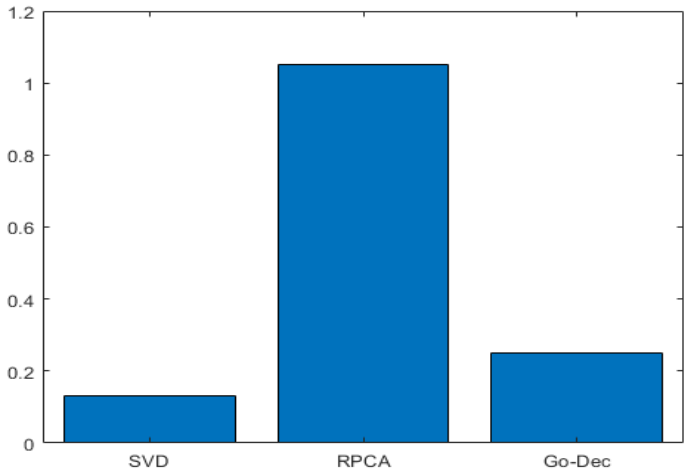

Figure 1. Computational time comparison of prescreening methods.

4.3. Feature Extraction

Ground reflection is removed, as described in Section 4.1. The Go Decomposition (GoDec) method is utilized for prescreening and is applied to all B-scan data, then the energy values of each A-scan are calculated, as shown in Figure 9.

$$X_E = \sum_{i=0}^{N} x(i)^2 \tag{8}$$

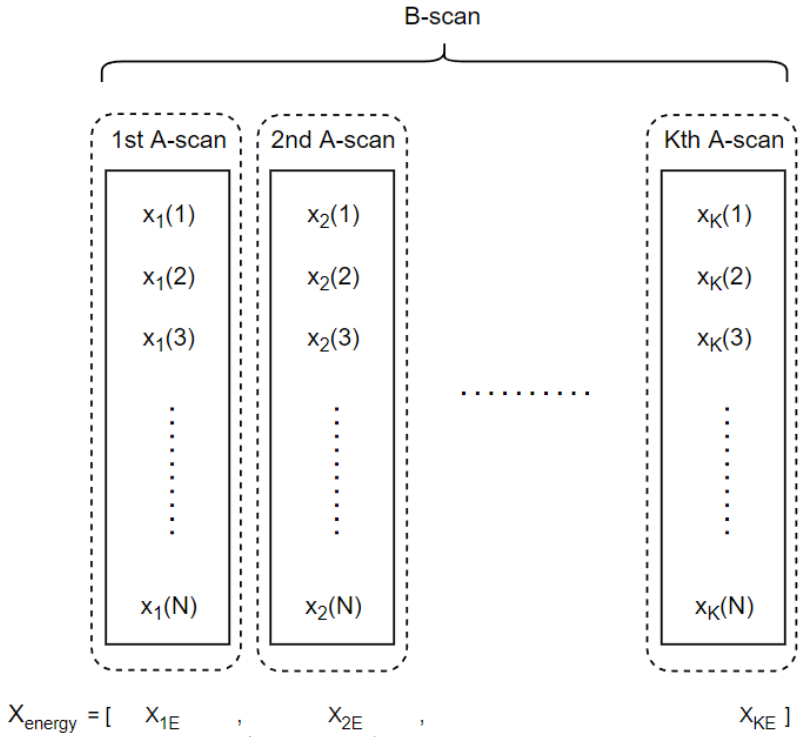

Figure 2. Creating a 1D energy vector.

This process is repeated for every B-scan, creating a 2D C-scan energy map. This work is shown in **Figure 3** for one scenario.

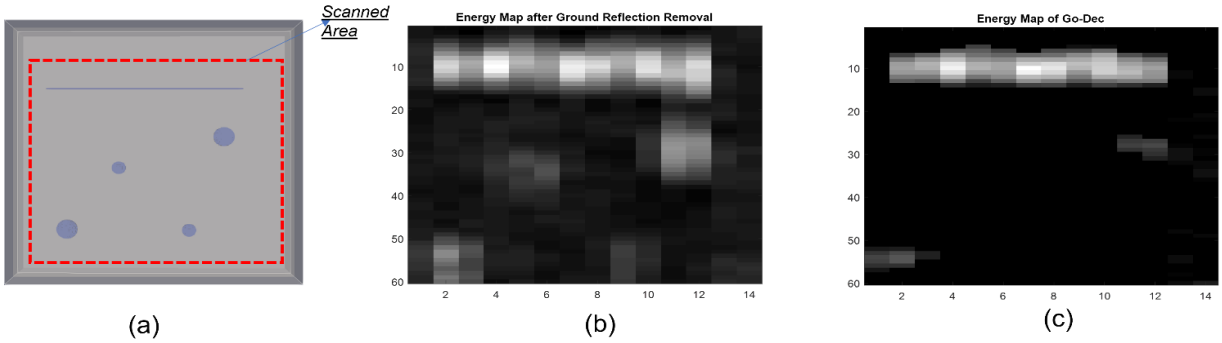

Figure 3. (a) Scenario with wire and clutter; (b) Energy map of ground reflection removal; (c) GoDec energy map.

After creating an energy map of the GoDec, a connected component analysis is utilized for image segmentation and feature extraction. Objects detected in the C-scan image are connected, and each is characterized as a single element using a connected component analysis.

The clustering method is studied for detecting an object and deciding whether it is a wire. For the clustering, there should be some features to utilize. Yılmaz [2] explains in detail which features might be used for wires. We use energy and the total number of binary detections. Based on these features, raw data of the simulation scenarios are shown in Figure 11. Feature datasets are normalized to avoid confusion.

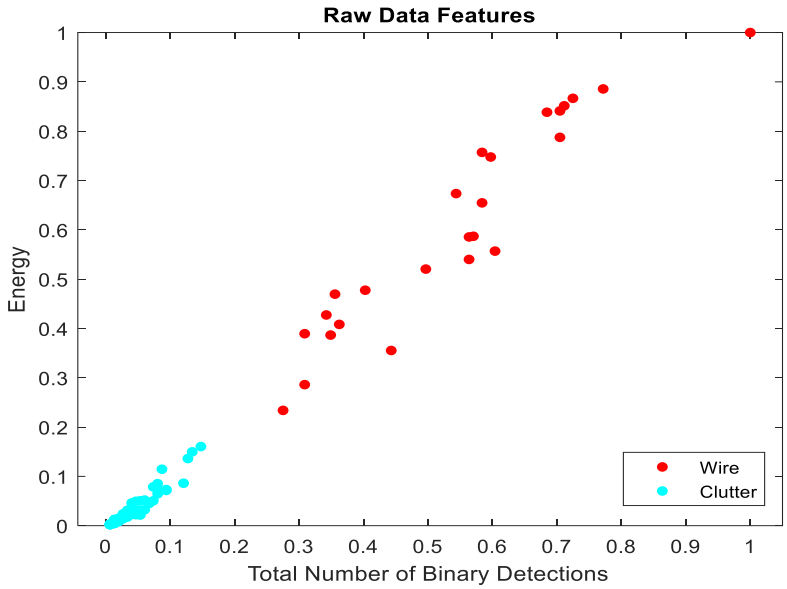

Figure 4. Raw features after GoDec.

4.4. Clustering

Clustering is an unsupervised machine learning technique that groups data for features. Since detecting IEDs is a dangerous but essential task, the target detection algorithm either must have 100% accuracy or should sound an alarm for objects that might be a target. In supervised learning, a training dataset is critical to discriminate and classify the anomaly. Since a wire can be in many different free forms, it is impossible to collect all the training data for buried wire in real life. Therefore, training in selected dataset features and classifying algorithms plays a critical role.

In this paper, the training dataset is created with different forms of wires and clutter. Features are extracted from the C-scan energy map and investigated with clustering algorithms. Features are grouped as clutter or target anomaly, and clutter is removed from the C-scan energy map. After these algorithms, the user should see the anomaly on a display unit and decide whether it is a target or not.

4.4.1. K-Means

The k-means algorithm is one of the most used clustering methods. This method groups the features by minimizing the total variance concerning cluster centroids. Clustering is performed by minimizing distances between *m* centroids and their corresponding assigned data points.

The distances between *m* centroids D_i (i=1,2,…..,m) and the n feature samples x_j (j=1,2,…..,n) are minimized as follows [21]:

$$min\Sigma_{i=1}^{m}\Sigma_{j=1}^{n}dist\left(x_j - D_i\right)^2 \quad (8)$$

The k-means clustering is a recursive algorithm that uses the iterative expectation maximization algorithm to determine the cluster membership that minimizes the sum of squared errors (SSE), as given in Equation (8). Firstly, given m, the number of clusters, the data points in the feature space are grouped into clusters with randomly initialized m centroids. In the next step, which is also called the expectation step (E-step), for each data point, the distance to each centroid is recomputed and each point is assigned to the cluster with the nearest centroid. Lastly, in the maximization step (M-step), the mean for each cluster is recompleted and the cluster centroids are updated. The k-means algorithm repeats the E-step and M-step until a convergence is reached. The convergence criteria can be defined as predetermined threshold values for distortions, maximum number of iterations, or when there is no change in cluster assignments [22].

4.4.2. Gaussian Mixture Model (GMM)

The GMM is used when the data distribution is unknown [23]. The GMM is an unsupervised clustering technique which is based on probability density estimations. It creates ellipsoidal-shaped clusters using expectation–maximization. The clusters are of a Gaussian distribution, always described by the mean and standard deviations. Using the mean and the covariance instead of only using the mean, as in the k-means, gives the GMM the ability to provide a better quantitative measure of fitness per number of clusters [22].

The GMM is a linear combination of Gaussian distributions and can be modeled as:

$$p(X) = \sum_{k=1}^{K} \pi_k N(X|\mu_k, \Sigma_k) \tag{9}$$

Where, K is the number of clusters in the model and π_k is the mixing coefficient, which is a density estimation for each Gaussian component also called clusters. $N(X|\mu_k, \Sigma_k)$ is the Gaussian density expressed as:

$$N(X|\mu, \Sigma) = \frac{1}{(2\pi)^{\frac{L}{2}}\sqrt{|\Sigma|}} exp\left\{-\frac{(X-\mu)^T\Sigma^{-1}(X-\mu)}{2}\right\} \tag{10}$$

where, μ is an L-dimensional mean vector, Σ is an L x L covariance matrix, and $|\Sigma|$ is the determinant of Σ.

The distance between data points and cluster centroids is calculated using Mahalanobis distance. The Mahalanobis distance is used widely in multivariate statistics applications. Euclidean distance differs because it considers the correlations between variables [24].

4.4.3. Comparison of Clustering Methods

Unsupervised algorithms perform based on the clusters they create. The performance of any unsupervised algorithms can change dramatically due to the wrong cluster number. Therefore, the first step is to decide the optimal number of clusters.

The elbow method, a famous visual cluster optimization method, is utilized to optimize the number of clusters. This method compares the difference in the sum of squared errors (SSE) of each cluster. The elbow angle's most extreme difference shows the best cluster number [25]. Evaluation of the best cluster number for the k-means is illustrated in Figure 12.

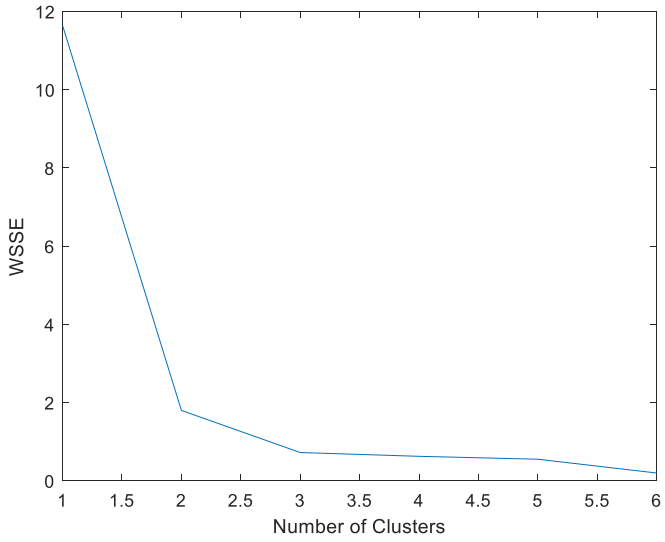

Figure 5. Evaluation of the best cluster number using the elbow method.

Table 1. Comparison of SSE differences with cluster numbers.

Number of Clusters	SSE	Difference of SSE
1	11.6410	-
2	1.7971	9.8439
3	0.7203	1.0768
4	0.6232	0.0971
5	0.5492	0.0740
6	0.1960	0.3531

It can be seen from Figure 12 and Table 1 that the most significant change occurs when there are two clusters. The difference between cluster 1 and cluster 2 is 9.8439. After that, all differences decrease slower from cluster 2. The clustering performance of the k-means algorithm with two clusters is illustrated in Figure 13.

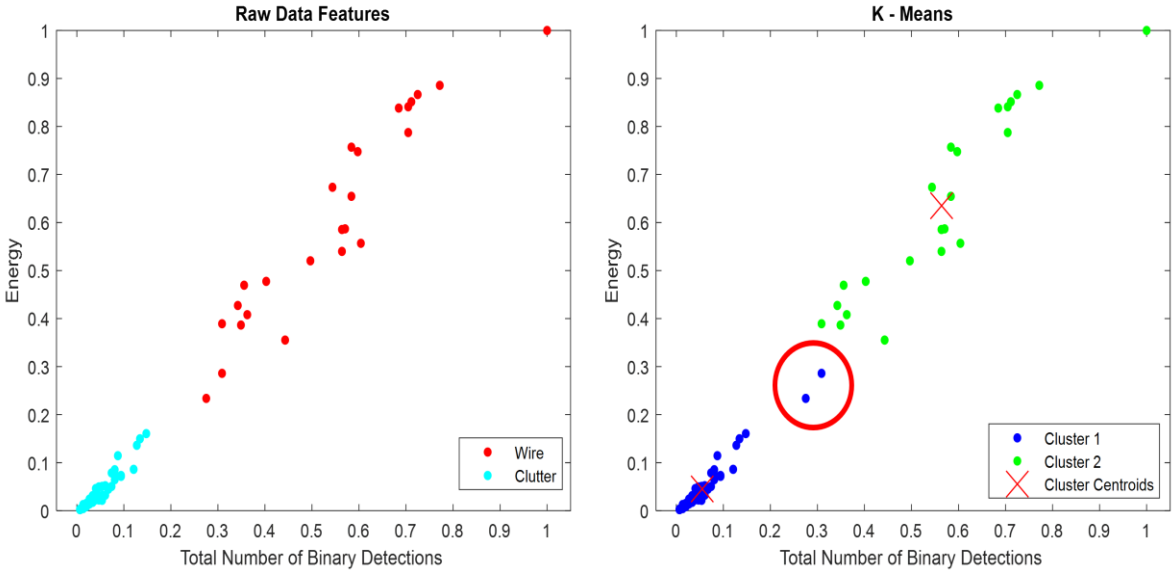

Figure 6. K-means clustering results.

Based on Figure 13, the k-means only clustered two data points wrongly out of 79, corresponding to a 97.47% accuracy. Information criterion tests are utilized to choose the best number of clusters for the GMM. The Akaike Information Criterion (AIC) and the Bayesian Information Criterion (BIC) are used to determine the clusters. The lower the AIC and BIC values, the more accurate the chosen clusters will be.

As described in the explanation of the GMM above, each Gaussian component uses the mean and the covariance matrices. The covariance matrix decides the shape and the orientation of the confidence ellipsoids. We can choose the covariance matrices of each component to be complete or diagonal and whether they share the same covariance matrix. Therefore, different covariance structures are evaluated with the AIC and BIC. The evaluation results are illustrated in Figure 14.

From Figure 14, it is clear that the AIC and BIC values decrease slower after two clusters. The full and unshared covariance matrix structures performed the best among other combinations. Figure 15 shows the visual results of the different covariance matrices on the feature dataset when the cluster number is two.

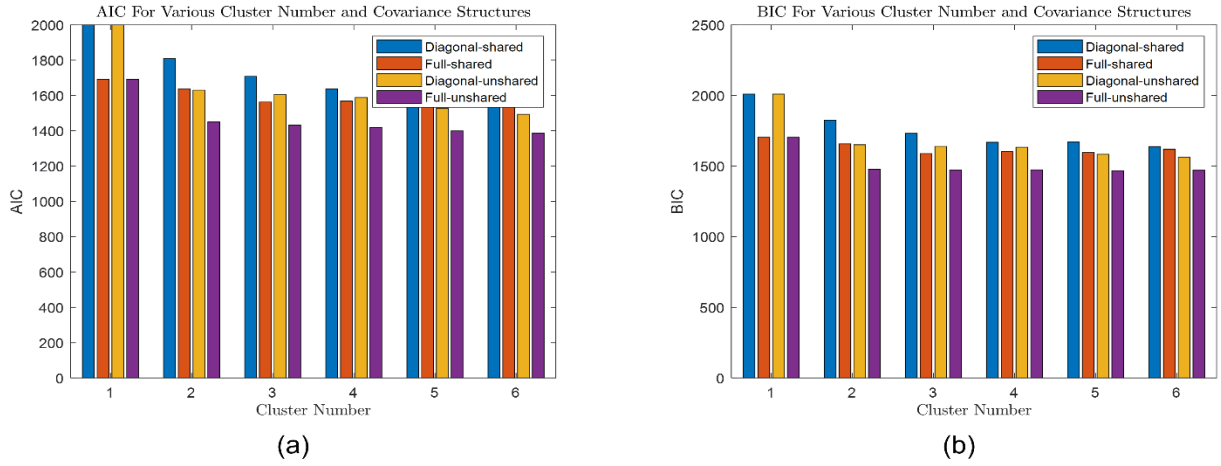

Figure 7. Evaluation of best cluster number: (a) AIC results with respect to different covariance structures; (b) BIC results with respect to different covariance structures.

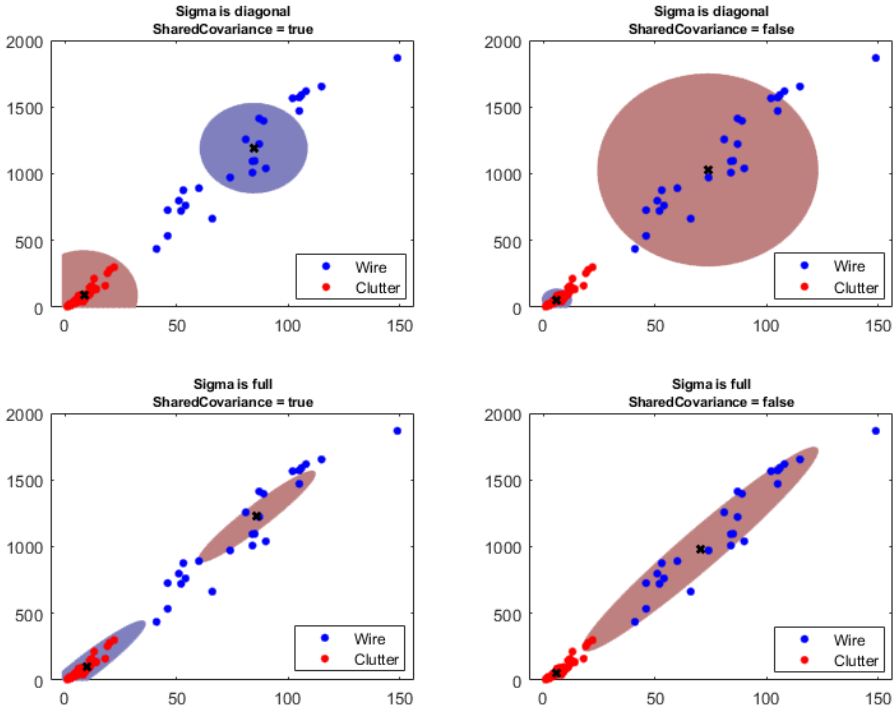

Figure 8. 95% confidence ellipsoids based on different covariance structures.

Confidence ellipsoids are drawn with 95% confidence. The GMM could not detect four wires and mis-detected three clutter points. If we increase the confidence level, then an increase would be seen in the volume of confidence ellipsoids, and the volume will decrease if the confidence level decreases. The clustering performance results of the GMM based on the confidence thresholds are compared for accuracy value, which is the ratio of the total number of accurate clustering to the total number of detections. The evaluation results are shown in Table 2.

Table 2. Accuracy results of the GMM with different thresholds.

Clustering with GMM, cluster number = 2			
	Threshold = 90%	**Threshold = 95%**	**Threshold = 99%**
Accuracy	92.41%	91.14%	87.34%

It is observed that increasing the threshold led to worse accuracy results. The increasing threshold of confidence ellipsoids led the GMM to detect the wires. However, it also detected clutter as wires. Decreasing the threshold overcomes the problem of detecting clutter as wires, but it also starts to miss wires.

The k-means clustering algorithm reached 97.47% accuracy. Therefore, in this study, we use the k-means clustering algorithm.

After comparing the prescreening and clustering algorithms, the flow of the proposed algorithms we used for cluster wire and clutter is shown in Figure 16.

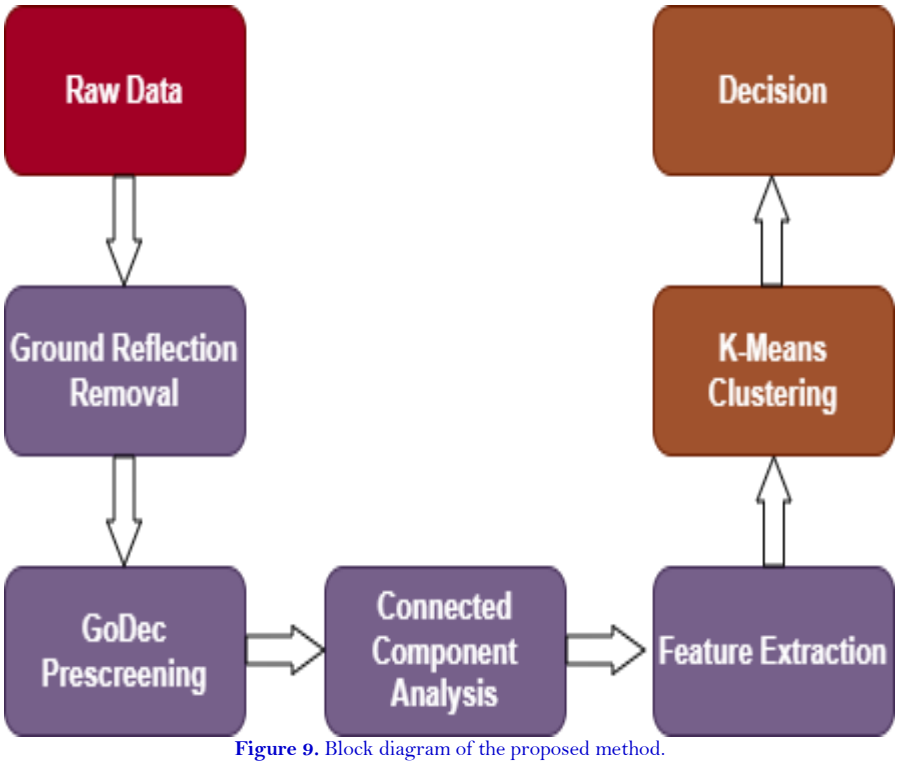

Figure 9. Block diagram of the proposed method.

5. SIMULATION RESULTS

Based on the algorithm flow in Figure 16, simulation results will be given in two different ways: raw simulation scenario and k-means clustering results. We decide whether the detected target is a wire or not based on k-means clustering. Thus, targets clustered as clutter will be deleted after the k-means algorithm, and only wires should be seen in the detection image. The simulation results are given in Figure 17 and Figure 18.

In the simulations, the GPR radar antenna polarization is defined as the X direction, which is identical to the cross-track direction. Thus, signals coming from other directions will be weakened drastically. This fact can be easily seen in scenarios 3, 6, 9, and 10. The two wrongly clustered data points circled in Figure 13 can be seen in the 15th and 18th scenarios.

Since the k-means calculates the distance based on Euclidean distance, the distance from these two data points is closer to the wire cluster centroid.

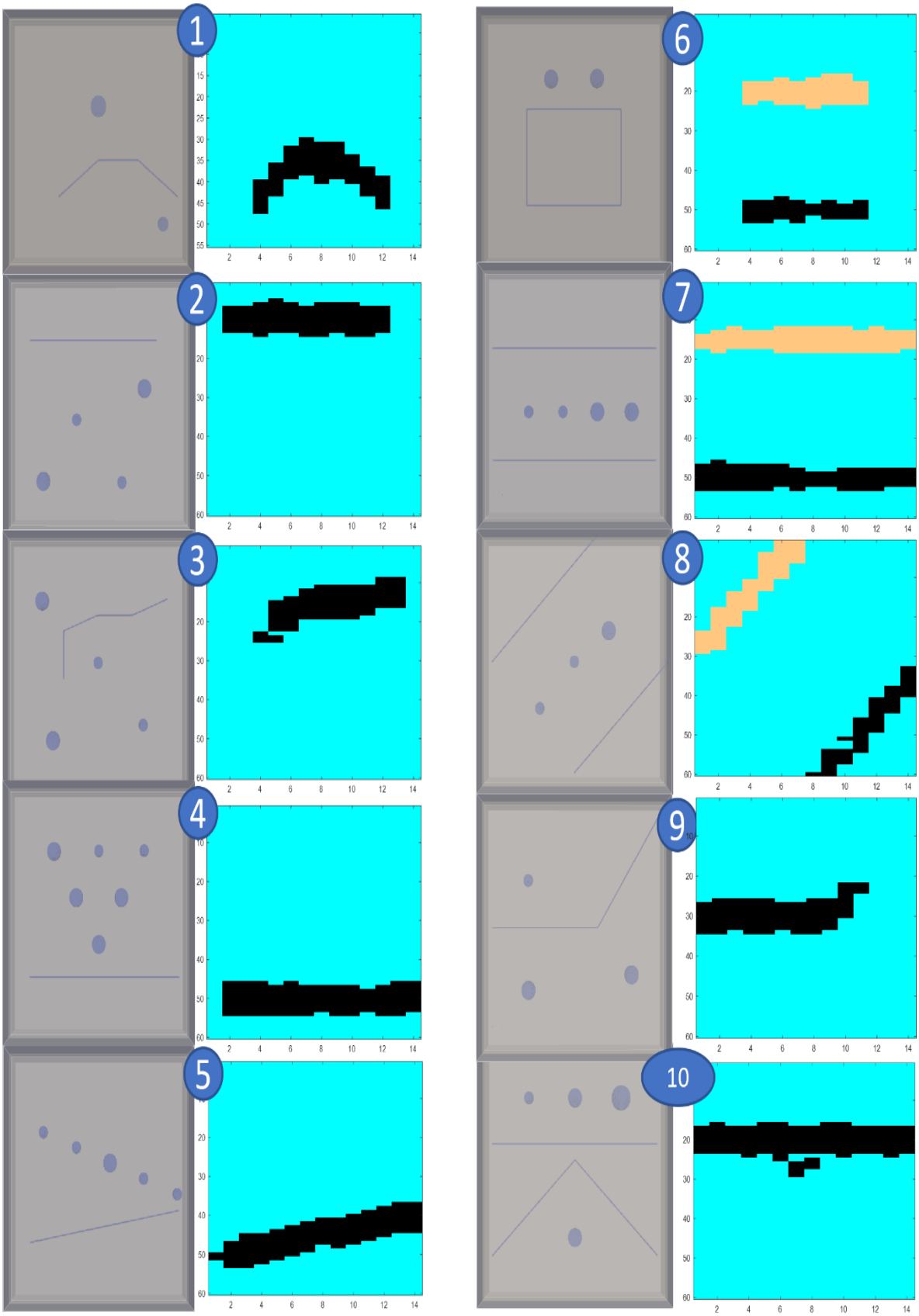

Figure 10. Scenarios from 1–10, and algorithm results.

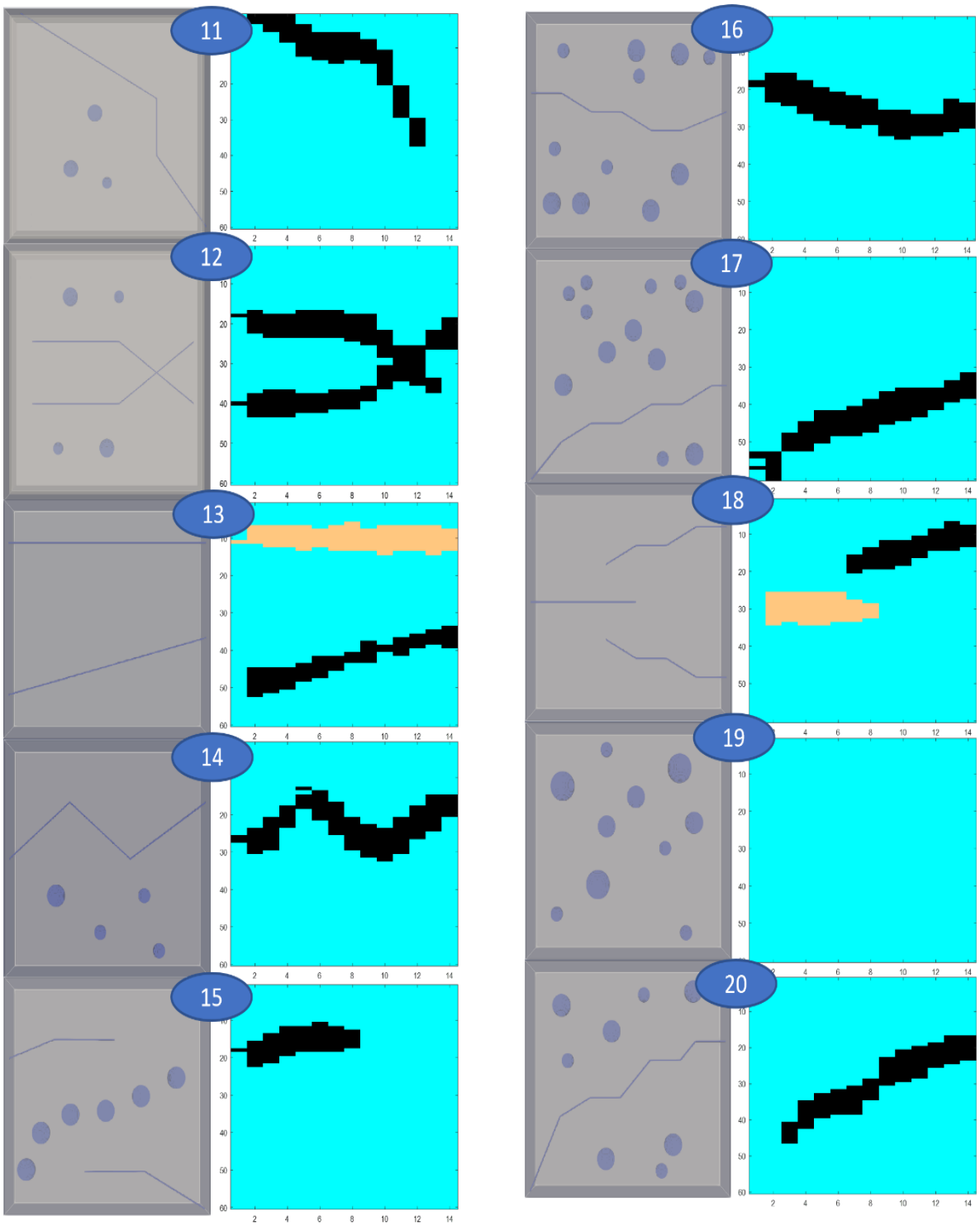

Figure 11. Scenarios from 10–20, and algorithm results.

6. CONCLUSION

In this study, we developed an algorithm for buried wire detection that is used to trigger IEDs. After ground bounce removal, the prescreening methods were studied and compared. The GoDec produced promising results both in computational time and SNR values. The k-means and GMM clustering techniques were also studied. Furthermore, the number of clusters is determined using the elbow method and the AIC and BIC methods. We compared different covariance structures for the GMM components, which determine the shape and the orientation

of the confidence ellipsoids. Also, different threshold values for confidence ellipsoids are compared. Since the distance of data points to the cluster centroids and the confidence ellipsoids are calculated with Mahalanobis distance, the data points out of these ellipsoids could not be detected. The k-means performed better than the GMM, with a 97.47% accuracy. Since the k-means uses Euclidean distance for distance calculation between data points and cluster centroids, its assignments were better for the featured dataset.

Funding: This study received no specific financial support.
Competing Interests: The authors declare that they have no competing interests.
Authors' Contributions: Both authors contributed equally to the conception and design of the study.

REFERENCES

[1] S. Colreavy-Donnelly, F. Caraffini, S. Kuhn, M. Gongora, J. Florez-Lozano, and C. Parra, "Shallow buried improvised explosive device detection via convolutional neural networks," *Integrated Computer-Aided Engineering*, vol. 27, pp. 403-416, 2020.Available at: https://doi.org/10.3233/ica-200638.

[2] U. Yılmaz, "Buried wire detection using ground penetrating radars," Masters Thesis Ankara Turkey Middle East Technical University, 2017.

[3] E. Temlioglu, I. Erer, and D. Kumlu, "A least mean square approach to buried object detection in ground penetrating radar," *Intrnational Geosci Remote Sens Symp*, pp. 4833–4836, 2017.Available at: https://doi.org/10.1109/igarss.2017.8128084.

[4] X. Liu, M. Serhir, and M. Lambert, "Detectability of junctions of underground electrical cables with a ground penetrating radar: Electromagnetic simulation and experimental measurements," *Construction and Building Materials*, vol. 158, pp. 1099-1110, 2018.Available at: https://doi.org/10.1016/j.conbuildmat.2017.10.038.

[5] C. Abeynayake and M. D. Tran, "Ground penetrating radar applications in buried improvised explosive device detection," in *Proceeding 2016 18th International Conference on Electromagnetic Devices. Advances in Applied ICEAA 2016*, 2016, pp. 564–567.

[6] I. Mesecan and I. O. Bucak, "Feature vector for underground object deteciton using B-scan images from GprMax," presented at the 2019 8th Mediterranean Conference on Embedded Computing, 2021.

[7] H. Liu, J. Zhao, and M. Sato, "A hybrid dual-polarization GPR system for detection of linear objects," *IEEE Antennas Wirel. Propag. Lett*, vol. 14, pp. 317–320, 2015.

[8] A. Heinzel, M. Peichl, E. Schreiber, S. Dill, and F. Bischeltsrieder, "Investigations on the detection of thin wires using MIMO SAR," presented at the In Detection and Sensing of Mines, Explosive Objects, and Obscured Targets, 2017.

[9] C. Warren, A. Giannopoulos, and I. Giannakis, "gprMax: Open source software to simulate electromagnetic wave propagation for ground penetrating radar," *Journal of Computational Physics Communication*, vol. 209, pp. 163–170, 2016.Available at: https://doi.org/10.1016/j.cpc.2016.08.020.

[10] A. Lalagüe, "Use of ground penetrating radar for transportation infrastructure maintenance," Doctoral Thesis at NTNU, 2015.

[11] M. M. Riaz and A. Ghafoor, "Ground penetrating radar image enhancement using singular value decomposition," *Proceeding-IEEE International Symptom Circuits Syst*, pp. 2388–2391, 2013.

[12] W. Xue, Y. Luo, Y. Yang, and Y. Huang, "Noise suppression for gpr data based on svd of window-length-optimized hankel matrix," *Sensors*, vol. 19, p. 3807, 2019.Available at: https://doi.org/10.3390/s19173807.

[13] F. H. C. Tivive, A. Bouzerdoum, and C. Abeynayake, "GPR target detection by joint sparse and low-rank matrix decomposition," *IEEE Trans Geosci Remote Sens*, vol. 57, pp. 2583–2595, 2019.Available at: https://doi.org/10.1109/tgrs.2018.2875102.

[14] M. P. Masarik, J. Burns, B. T. Thelen, J. Kelly, and T. C. Havens, "GPR anomaly detection with robust principal component analysis," in *In Detection and Sensing of Mines, Explosive objects, and Obscured targets XX*, 2015, pp. 395-405.

[15] E. J. Candès, X. L. Ma, Y., and J. Wright, "Robust principal component analysis?," *Journal Association for Computing Machinery*, vol. 58, pp. 1-37, 2011.

[16] X. Song, D. Xiang, K. Zhou, and Y. Su, "Improving RPCA-based clutter suppression in GPR detection of antipersonnel mines," *IEEE Geoscience and Remote Sensing Letters*, vol. 14, pp. 1338-1342, 2017.

[17] X. Song, D. Xiang, K. Zhou, and Y. Su, "Fast prescreening for GPR antipersonnel mine detection via go decomposition," *IEEE Geoscience and Remote Sensing Letters*, vol. 16, pp. 15-19, 2019.

[18] T. Zhou and D. Tao, "GoDec: Randomized low-rank & sparse matrix decomposition in noisy case," presented at the Proceedding 28th International Confrence Machine Learning ICML, 2011.

[19] J. Li, Y. Huang, G. Liao, and J. Xu, "Moving target detection via efficient ATI-GoDec approach for multichannel SAR system," *IEEE Geoscience and Remote Sensing Letters*, vol. 13, pp. 1320-1324, 2016.Available at: https://doi.org/10.1109/lgrs.2016.2584083.

[20] M. Welvaert and Y. Rosseel, "On the definition of signal-to-noise ratio and contrast-to-noise ratio for fMRI data," *PLoS One*, vol. 8, p. e77089, 2013.Available at: https://doi.org/10.1371/journal.pone.0077089.

[21] C. Völker and P. Shokouhi, "Clustering based multi sensor data fusion for honeycomb detection in concrete," *Journal of Nondestructive Evaluation*, vol. 34, pp. 1-10, 2015.Available at: https://doi.org/10.1007/s10921-015-0307-7.

[22] E. Patel and D. S. Kushwaha, "Clustering cloud workloads: K-means vs gaussian mixture model," *Procedia Computer Science*, vol. 171, pp. 158-167, 2020.

[23] R. Tilley, H. R. Sadjadpour, and F. Dowla, "GPR imaging for deeply buried objects: A comparative study based on compositing of scanning frequencies and a chirp excitation function," *Geosciences*, vol. 9, pp. 1-23, 2019.Available at: https://doi.org/10.3390/geosciences9030132.

[24] H. Ghorbani, "Mahalanobis distance and its application for detecting multivariate outliers," *Facta Universitatis-Series Mathematics and Informatics*, vol. 34, pp. 583-595, 2019.Available at: https://doi.org/10.22190/fumi1903583g.

[25] E. Umargono, J. E. Suseno, and S. K. Vincensius Gunawan, "K-means clustering optimization using the elbow method and early centroid determination based-on mean and median," in *Proceedings of the International Conferences on Information System and Technology*, 2020, pp. 234–240.